

Contents lists available at ScienceDirect

# Ocean Modelling

journal homepage: www elsevier com/locate/ocemod



# River plume source-front connectivity

Kelly L. Cole a,\*, Daniel G. MacDonald b, Georgia Kakoulaki c, Robert D. Hetland d

- <sup>a</sup> Department of Civil and Environmental Engineering, University of Maine, Orono, ME, USA
- <sup>b</sup> Civil and Environmental Engineering, University of Massachusetts-Dartmouth, Dartmouth, MA, USA
- c Department of Estuarine and Ocean Sciences, School for Marine Science and Technology, University of Massachusetts-Dartmouth, New Bedford, MA, USA
- <sup>d</sup> Department of Oceanography, Texas A M University, College Station, TX, USA



Keywords: Coastal ocean modeling Buoyancy driven flow River plumes

### ABSTRACT

River plume source-front connectivity, or the relationship between processes at the source, plume body and front, is investigated with numerical simulations of the Merrimack River plume using the Regional Ocean modeling System (ROMS). Source water, i.e. water discharged from the estuary during an ebb pulse, overtakes the front as it propagates offshore, resulting in the strong convergence that exists there. Model results show that much of the water released over an ebb pulse does not interact with the propagating tidal plume front, suggesting that the front decouples from the source and sustains itself as a distinct water mass. When a gate is closed at the estuary mouth during early ebb, the overall plume structure changes; gates closed late in ebb do not significantly effect the along- or cross-shore scale of the plume. The change in plume extent is only evident hours after the early-ebb gate closing, when source water is no longer supplied to the front. These experiments suggest that the growing distance between the highly energetic liftoff region and the radial expansion of the plume front results in a flattening of the surface gradient driving flow in the interior, diminishing source-front connectivity.

## 1 Introduction and background

Temporal variability of fresh water discharge from estuaries is an important element of the physical environment that shapes coastal ecosystems. In tidally modulated regions, buoyant water of riverine origin is pulsed from an estuary mouth onto the shelf during the ebb tide. The buoyant water shoals and spreads over dense receiving shelf water, creating an energetic shear mixing region (Hetland and MacDonald, 2008). The plume spreads offshore as the ebb progresses, and accumulations of nutrients, plankton and other materials may be trapped and transported in the seaward boundary of each ebb pulse by the strong convergence that exists there (Scotti and Pineda, 2007). The seaward boundary separating the discharge from ambient ocean water is the frontal region of the river plume. The interaction between source water and ambient shelf water is amplified at the tidal plume front; recent studies estimate that in some estuary-shelf systems, the tidal plume front is where a large portion of source water mixing from fresh to ocean salinities takes place (Orton and Jay, 2005; Pritchard and Huntley, 2006).

Similar to the plume behind it (Horner-Devine et al., 2015), the front undergoes a transition on tidal time scales from a non-rotational to a geostrophic phenomenon. Near the source, where the density anomaly and velocity of the outflow strongly affect plume evolution, a

convective, bore-like structure is observed at the front as it emerges into the coastal ocean (Marmorino and Trump, 2000). The frontal region is characterized by a convergence zone and turbulent wake, plunging to a depth several times deeper than the plume behind it (Kilcher and Nash, 2010). By the end of the tidal cycle, when the front is a great distance away from the mouth, the structure of the plume front has begun a transformation towards geostrophy, and a structure with many similarities to a shelf-break front in cross-shore thermal wind balance with reduced vertical mixing (e.g. Yankovsky and Chapman (1997)). Thus, it is expected that river plume source-front connectivity, or the relationship between processes at the source, plume body and front, will exhibit variability over the ebb tide phase. Previous studies focus on dynamics near the river mouth (e.g., Hetland (2005), MacDonald et al. (2007), Hetland (2010) and Kilcher et al. (2012)) or the structure of the plume front (e.g., Marmorino and Trump (2000) and Jay et al. (2010)), but few studies examine the connection between both regions that we will address in this study. Early plume models (Garvine, 1982, 1987) allow information from the front to travel into the plume along characteristics so that processes at the front establish the structure of the plume body. A key theme of these model results, and many models that evolved from the Garvine series, is plume connectivity and a better understanding of the interaction between the plume front

E-mail addresses: kelly.cole@maine.edu (K.L. Cole), dmacdonald@umassd.edu (D.G. MacDonald), georgia.kakoulaki@gmail.com (G. Kakoulaki), hetland@tamu.edu (R.D. Hetland).

<sup>\*</sup> Corresponding author.

and plume interior structure. Although qualitatively useful, these early models fall short in their ability to reproduce many details of the frontal region because of initial assumptions made about the front structure (O'Donnell et al., 1998).

The goal of this study is to quantify the amount of source water, or water released from the estuary over a single ebb pulse, that interacts with the tidal plume front. This information has been overlooked in previous studies that evaluate total plume mixing at the front through comparison of mixing measurements at the front with fresh water flux at the source.

The importance of the front to overall plume structure. Communication between the mouth and the front is achieved through source water traversing the plume and overtaking the front (Garvine and Monk, 1974; O'Donnell et al., 1998; Marmorino and Trump, 2000; Kilcher and Nash, 2010). Previous laboratory studies of gravity currents and observational studies of buoyant plumes show that fresh water leaves the source, travels through the core of the plume and is cycled through the front; this supply of buoyant water to the front is necessary to sustain frontal propagation throughout ebb. Despite early studies highlighting the importance of fronts and their potential for coastal water mass modification (Garvine and Monk, 1974; Garvine, 1982, 1987; Luketina and Imberger, 1987; Chen, 1980), the role of frontal processes in plume evolution is still not well understood. Recent studies highlight processes at the source, near-field or front separately, but the relative importance of each region to plume propagation is unclear. Hetland (2010) investigates the effect of inflow variables on plume interior mixing to determine expansion; the details of frontal dynamics are overlooked. Results from MacDonald et al. (2007) and Hetland and MacDonald (2008) suggest that g' at the front is set by interior mixing as frontovertaking waters traverse the plume. Alternatively, Jay et al. (2010) assumes local frontal dynamics are responsible for the advancement of the plume, removing interior plume dynamics in an analytical modeling study. Kilcher and Nash (2010) link ebb discharge at the estuary mouth to frontal propagation, however, they do not examine the path of source water through the plume core in detail.

Engineering studies applied to the fronts steady propagation phase. The front has a convective head structure during the steady propagation phase (Luketina and Imberger, 1987; Marmorino and Trump, 2000; Kilcher and Nash, 2010) that can be related to engineering scale gravity currents in a tank or small scale environmental scenarios (Benjamin, 1968; Huppert and Simpson, 1980; Rottman and Simpson, 1983; Chen and MacDonald, 2006). Frontal processes have been explored in engineering scale studies that, ignoring the difference in aspect ratio, are comparable to geophysical scale studies. The anatomy of the current is fairly consistent across laboratory studies, composed of a head region of uniform velocity, a dissipative wake region where velocity is nonuniform and greater than the front speed, exhibiting Kelvin-Helmholtz billows generated at the head; often a tail region is also identified where mixing and overtaking velocities diminish (Lowe et al., 2002; Marino et al., 2005). A contribution of many studies is the development of formulae to predict frontal Froude number ( $Fr_f = \overline{g'h}$ ), where g'is the reduced gravity and h is the plume depth, using characteristics of the flow at and around the head of the current; these measures are somewhat difficult to extrapolate to geophysical flows (Huppert and Simpson, 1980; Rottman and Simpson, 1983). Theoretical values of frontal Froude number are well established for the constant velocity phase and tend to be O(1). Benjamin (1968) determines  $Fr_f \sim$ using inviscid theory, and is fairly accurate in prediction of river plume front speed, suggesting that the head of the current is relatively unaffected by the complicated flow trailing the front (e.g. Jay et al. (2010)).

Importance of frontal mixing to the total mixing of estuarine discharge. A variety of studies have evaluated mixing within a plume front and in some cases attempted to extrapolate from these observations the importance of frontal mixing to the plume as a whole. Luketina and Imberger (1987) measure a Richardson number consistent with turbulent mixing up to 300 m behind the front in a small, tidally pulsed plume. Orton and Jay (2005) suggest that a 100 m zone behind the front is responsible of mixing in the Columbia River tidal plume (measured dissipation  $\sim 10^{-4}$  m<sup>2</sup> s<sup>-3</sup>), though their measurements were later in ebb and extrapolated much more broadly. Pritchard and Huntley (2006) suggest that mixing at the front of a small discharge entering tidally energetic waters is strong enough that a plume does not form 65 the time during spring tides because plume water is mixed to ambient salinity by frontal processes during its early formation. A goal of this study is to quantify the fraction of total source water that interacts with the front, which will have implications for the importance of frontal mixing to the total ebb discharge.

#### 2 Model and methods

Realistic and idealized numerical simulations of the Merrimack River estuary–shelf system are used in this study. The Merrimack is a medium discharge river (typically 300–700  $\rm m^3~s^{-1})$  that empties into the Gulf of Maine; it is an ideal location to study plume properties because of a narrow estuary mouth and uncomplicated coastal geometry.

The Regional Ocean Modeling System (ROMS) (Shchepetkin and McWilliams, 2005), a hydrostatic, sigma-coordinate model, is paired with a curvilinear grid that represents the Merrimack River estuary and shelf region on the coast of Massachusetts and New Hampshire (Fig. 1). The grid spans the head of the Merrimack estuary to  $\sim$ 20 km offshore, and ranges from ~10 km upcoast of the estuary mouth to Cape Ann, ~20 km downcoast of the mouth. Near-field mixing rates and flow characteristics have been validated in this model and it is applied in Hetland and MacDonald (2008) and Chen et al. (2009). The offshore boundary is moved farther offshore in these simulations to ensure the plume is contained in within the domain. Cole (2014) presents further comparison of model simulated fields with the shipboard, high-sampling-frequency CTD tow-yow transects through the core of the plume described in MacDonald et al. (2007). Fig. 2 shows some examples of these comparisons. All data are linearly interpolated to a grid with 40 m spacing in the offshore direction and 0.25 m in the vertical. In general, the model represents the plume lift off point well and the location of the core of fresh water during late ebb. The model compares to data best in interior plume stratification and plume depth during high discharge, but performs well over the range of forcing during 2006/2007 freshet.

The model has 30 vertical layers and the spatial resolution ranges from  ${\sim}40$  m at the mouth to  ${\sim}100$  m at the offshore boundaries. The width and average depth at the mouth is 276 m and 6.3 m respectively and the model bathymetry includes a shallow bar  ${\sim}300$  m seaward of the estuary mouth where fresh water loses contact with the bottom during plume formation. Fresh water enters the domain  ${\sim}10$  km up the river from the estuary mouth. It generally takes less than 12 h for a parcel of water to travel the length of the estuary and enter the coastal ocean.

The model uses MPDATA vertical and horizontal tracer advection (Smolarkiewicz and Clark, 1986). Tracers are horizontally mixed along geopotential surfaces. Vertical mixing is described by k- $\epsilon$  turbulence closure coupled with Canuto A-stability function formulation (Canuto et al., 2001). Horizontal smoothing of buoyancy and shear is implemented. Quadratic bottom friction is incorporated into the momentum equation and conservative, parabolic spline reconstruction is used for vertical derivatives in the model. A Flather boundary condition (Flather, 1976) is used for 2-D velocity components and the free surface and an Orlanski boundary condition is used for 3-D

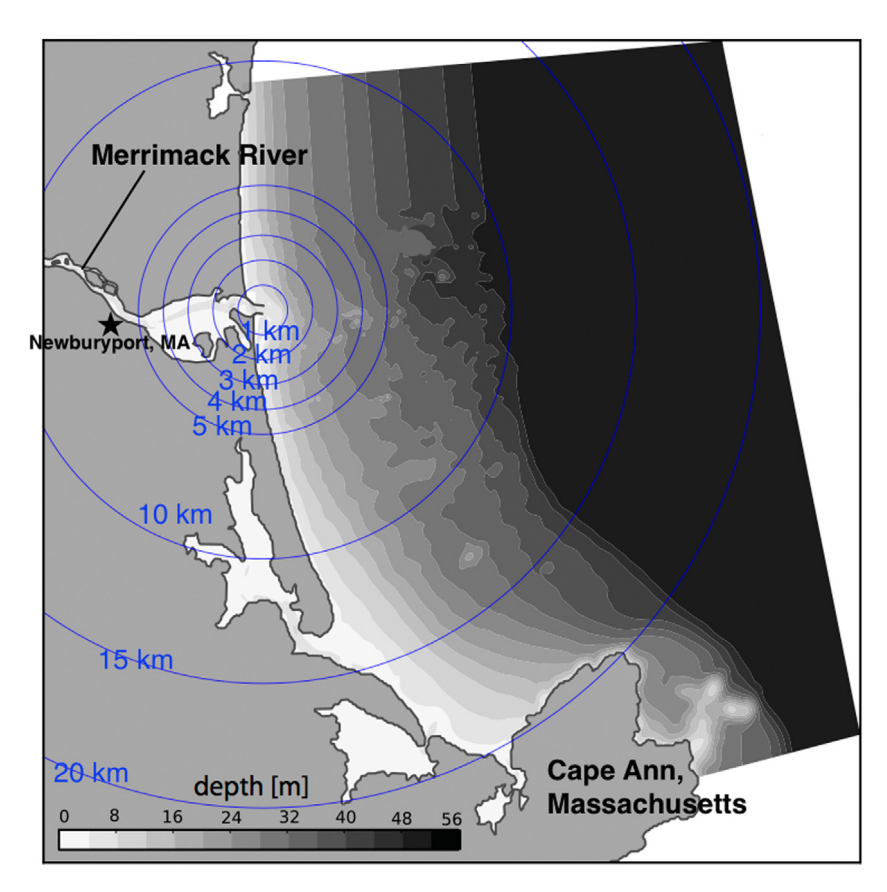


Fig 1 Merrimack River estuary and shelf domain. Blue lines show distance from the Merrimack estuary mouth. Grid spans approximately 10 km up the estuary from the mouth to 20 km offshore into the Gulf of Maine.

velocity components and tracers at the north, east, and south open boundaries (Orlanski, 1976).

For realistic simulations, domain wide wind forcing is applied from a NOAA meteorological station at the Isle of Shoals, ~25 km northeast of the estuary mouth. River discharge used in the model is recorded by the USGS at a hydrologic unit at Lowell, MA. A southward flowing  $\sim$ 5 cm s<sup>-1</sup> ambient coastal current is applied at the northern open boundary. Waters in the Gulf of Maine follow a seasonal cycle with fall/winter convection from surface to mid-water column, six major river inflows in spring, and restratification in summer. The Saint John, Penobscot and Kennebec Rivers are located upcoast of the Merrimack River, all with larger discharges influencing the coastal current system. The core of the Western Maine Coastal Current is typically 2 psu below the ambient salinity,  $\sim 0.2 \text{ m s}^{-1}$  and can be located  $\sim 40$ km offshore, however, this transport significantly diminishes between Penobscot bay and the Merrimack estuary. The early tidal evolution of the Merrimack plume, which is the focus of this modeling study, is generally more sensitive to residual shelf stratification caused by advection and mixing of past tidal pulses than the Gulf of Maine coastal current system (i.e. forced internally from within the domain rather than entering at the open boundaries). More details about the ambient ocean conditions can be found in Geyer et al. (2004) and summarized in Cole (2014).

A  $\sim$ 1.5 m semidiurnal tide is forced at the open boundaries by the free surface. Xtide (Flater, 2005), a harmonic tide clock and time predictor software, is used to create forcing. XTide uses the same algorithm to predict tides as the US Nation Ocean Service and the prediction at the 'Plum Island, Merrimack River Entrance, Merrimack River, Massachusetts' station is used here. The tidal phase is referenced to the sea surface height at the estuary mouth in the analyses presented in this paper. Estuarine outflow typically starts before high water and generally persists longer than six hours in the simulations. Modeled physical parameters at the river mouth are presented in Fig. 3. Gray

regions highlight tidal cycles analyzed in this study and Fig. 4 shows surface salinity every  $\sim 0.5$  h over the indicated tides. The model is initialized with a background ocean salinity and temperature field. The entire model simulation spans the months of April and May 2011. The Merrimack estuary is a strongly time dependent salt wedge (Geyer et al., 2008; Ralston et al., 2010) that spins up quickly, especially during freshet. The first dye and particles are released 27 days after initialization to ensure a realistic estuarine initial condition. Realistic ambient stratification in the region near the river mouth is established once the estuary is steady by the older tidal pulses on the shelf.

Location of the tidal plume front is determined by 1000 numerical surface drifters released in an arc behind the front when it emerges from the estuary mouth (typically slightly before high water). The drifters stay with the front as the plume spreads offshore. Since the drifters spread apart as time passes, the front is linearly interpolated where the distance between drifters is more than 300 m. Fig. 5 shows surface convergence in the plume at four times during an ebb pulse (tide A in Fig. 3). Fronts exhibit high convergence. The front marked by the drifters (red line) follows the primary front shown in the surface convergence during ebb. Therefore, the drifters provide a reasonable location of the tidal plume front.

Lagrangian tracking is coded in post-processing of the model simulation. The surface plume velocity field is used to propagate particles forward in time from:

$$u_0 = x_1 - x_0)/\Delta t \tag{1}$$

$$v_0 = y_1 - y_0)/\Delta t \tag{2}$$

where  $u_0$ ,  $v_0$ ,  $x_0$  and  $y_0$  are the velocities and particle positions at the current time step,  $x_1$  and  $y_1$  are the particle positions at the next time step and  $\Delta t$  is the time step for offline particle tracking (which can be greater than the ROMS internal time step). Several values of  $\Delta t$  were tested with a final choice of  $\Delta t = 3$  min tracking the front well. ROMS

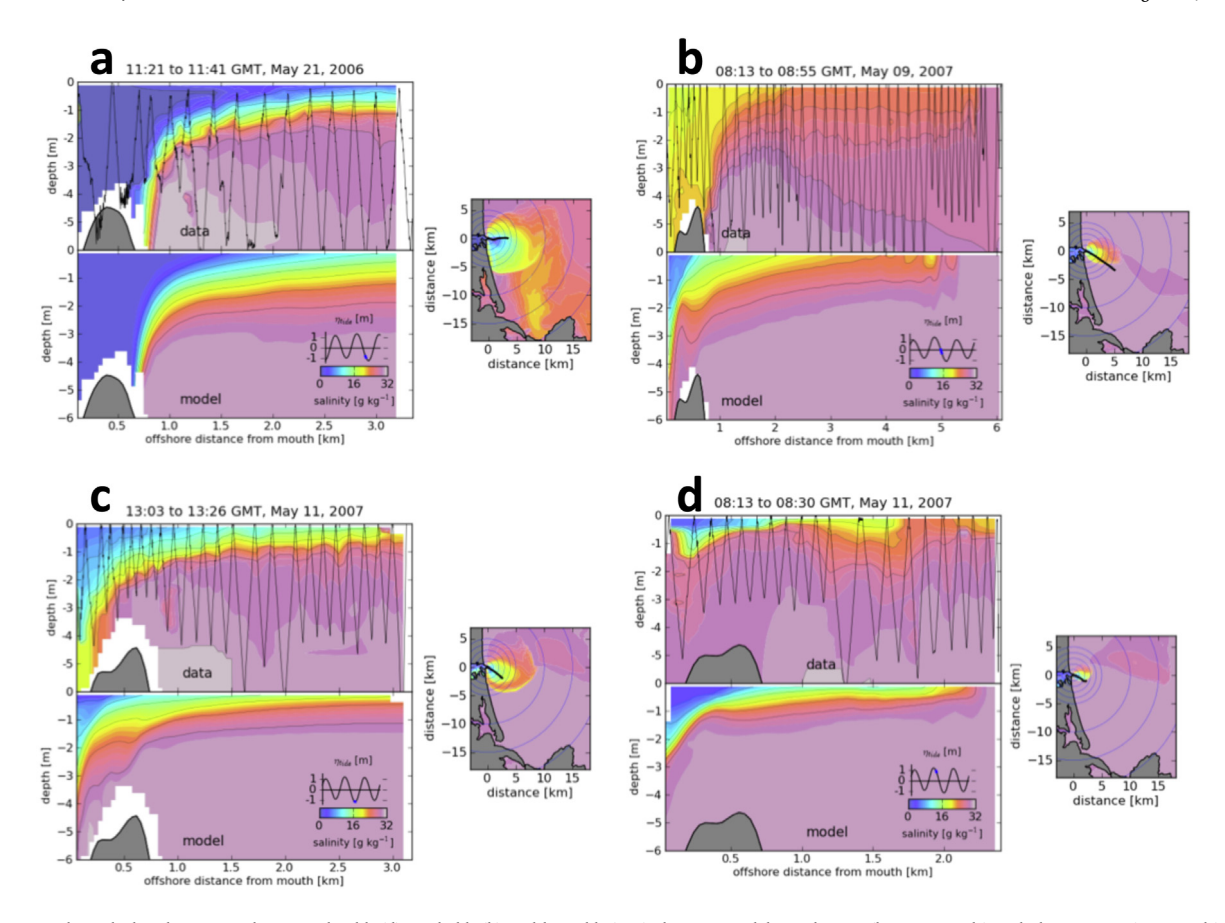


Fig 2 Transects through the plume core during early ebb (d), mid-ebb (b) and late ebb (a, c) showing model simulations (bottom panels) and observations (top panels) of salinity. Black lines in the data panels show the CTD position. Location of the transect and modeled surface salinity during the transect is shown on right.

Source: From Cole (2014).

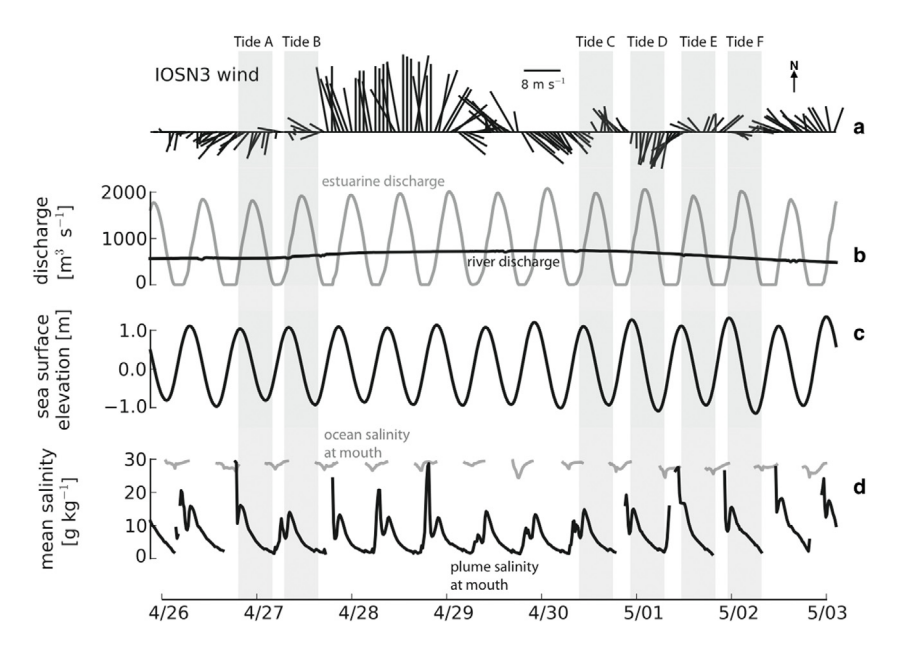


Fig 3 (a) Wind forcing during simulation, (b) river inflow into the domain and estuarine discharge into the ocean part of the domain, (c) sea surface elevation at a grid cell at the river mouth, (d) mean salinity of outflowing (plume) water into the ocean and inflowing (ocean) water into the estuary.

modeled fields are saved approximately every fifteen minutes, so the particle tracks are interpolated over this time. Starting locations of the drifters are spaced across the mouth such that the particles do not overlap initially and no two drifters follow the same path. Since there is realistic variability amongst the drifter tracks, no overlap, and good

resolution along the front from north to south, no artificial diffusion is added to the particle tracking scheme.

Source water pathways are investigated using surface drifter clusters and passive dye tracers released at the estuary mouth during tides A, B, C, D, E and F. We focus high frequency dye release experiments

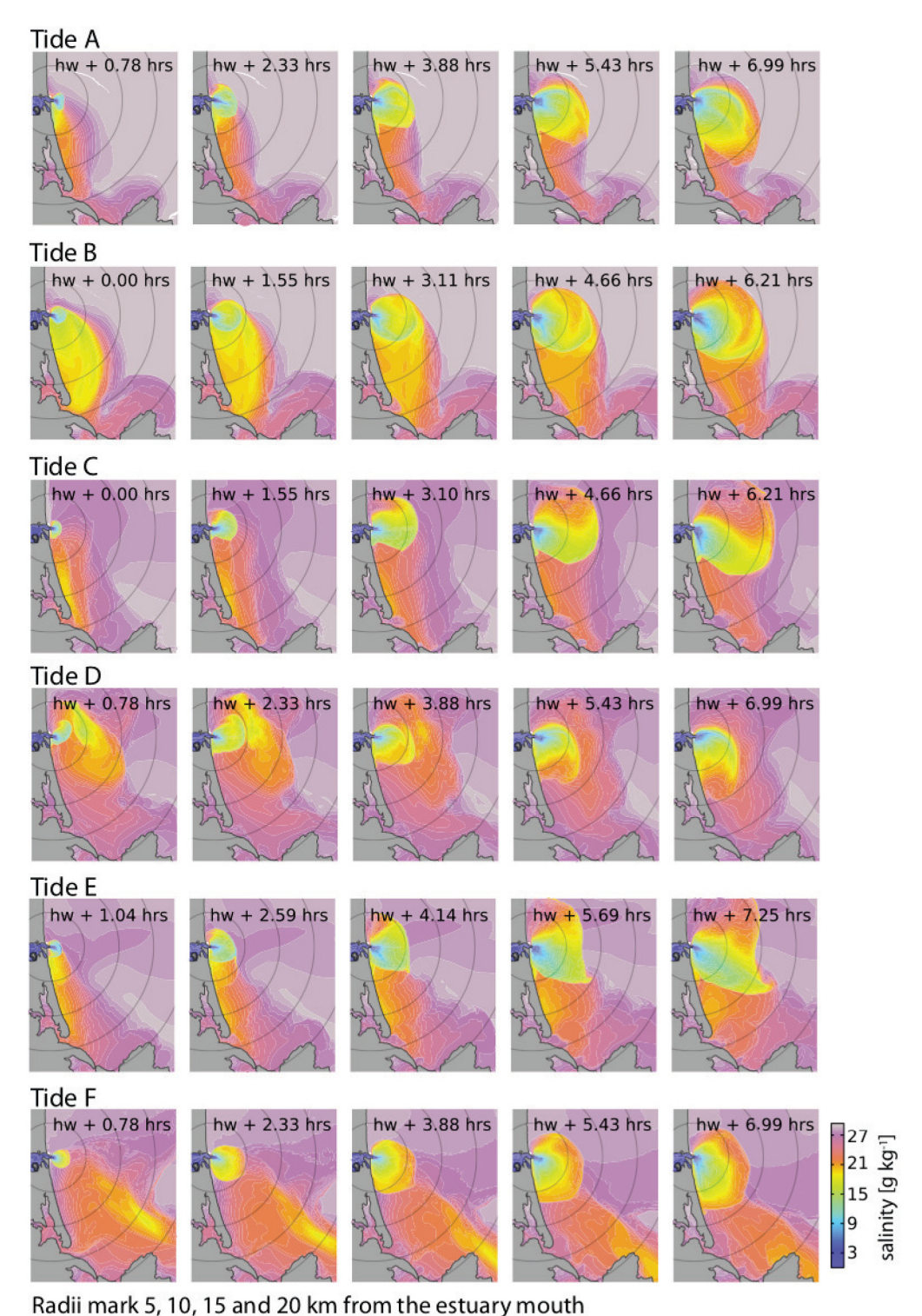


Fig 4 Time sequences of sea surface salinity over the ebbs highlighted in Fig. 3. 'hw' is 'high water' (i.e. high slack tide).

on the first of the back-to-back tides (A, C and E). Tide A illustrates a classic downcoast turning bulge and tide C presents a relatively radial plume expansion case, so they are explored in more detail. Dye tracers are released full water column at the mouth to study dilution of source water traversing the plume. The experiments presented in this research are listed in Table 1. A coastal wall is added to the grid at the estuary mouth at mid-ebb in the gate experiments described in Table 1, damming estuarine discharge. This is achieved by running the original grid into ebb, stopping the simulation during ebb and using the final

simulated fields to initialize a new grid with a wall at the estuary mouth to complete the ebb simulation.

## 3 Results

# 3.1. How much source water reaches the plume front?

We consider how much dye interacts with the front over the first six hours of ebb, starting when the front emerges from the estuary

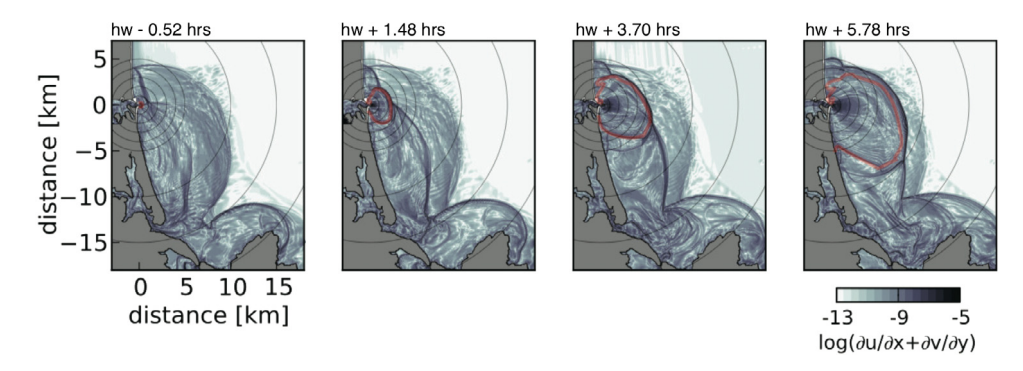


Fig. 5 Evolution of tide A labeled in Fig. 3. Panels are approximately two hours apart. Blue contours show log of surface convergence. The red line identifies the location of the front.

**Table 1**Dye release experiments in the Merrimack simulations. All dyes are released full water column at grid cells spaced 40 m apart across the estuary mouth (at the end of the jetties). 'Start of ebb' is the time step (relative to high water) when the tidal plume front emerges from the estuary mouth and drifters are released to mark the front position.

Experiment	Tide	Start of ebb	Start of release	No. dyes released	Release frequency	Release duration	Gate closing time
A1	2nd ebb, 4/26/11	-0.52 h	-0.52 h	1	Throughout ebb	6 h	_
B1	1st ebb, 4/27/11	-1.29 h	-1.29 h	1	Throughout ebb	6 h	_
C1	1st ebb, 4/30/11	−1.29 h	-1.29 h	1	Throughout ebb	6 h	-
D1	2nd ebb, 4/30/11	-0.52 h	-0.52 h	1	Throughout ebb	6 h	-
E1	1st ebb, 5/1/11	-0.26 h	-0.26 h	1	Throughout ebb	6 h	-
F1	2nd ebb, 5/1/11	-0.52 h	-0.52 h	1	Throughout ebb	6 h	-
A3	2nd ebb, 4/26/11	-0.52 h	+0.00 h	3	Every 2 h	1 h	-
C3	1st ebb, 4/30/11	−1.29 h	-0.77 h	3	Every 2 h	1 h	-
E3	1st ebb, 5/1/11	-0.26 h	+0.27 h	3	Every 2 h	1 h	_
A12	2nd ebb, 4/26/11	-0.52 h	-0.52 h	12	Every 30 min	30 min	_
No gate	2nd ebb, 4/26/11	-0.52 h	-0.52 h	1	Throughout ebb	6 h	_
Gate	2nd ebb, 4/26/11	−0.52 h	−0.52 h	1	During early ebb	1.3 h	+ 0.78 h

mouth. This timing is offset from high water and the duration of ebb outflow varies, as expected in a realistically forced model. We analyze several ebbs during the early, steady propagation frontal phase (Kilcher and Nash, 2010). Note that some quantity of all dyes released interact with the front – even dyes released late in ebb – if given enough time. However, once the plume (and front) has assimilated into older plume waters, the interaction is not relevant to source-front connectivity as we have defined it.

Surface dye concentrations and vertical structure over a cross-shore transect are given in Fig. 6 for tide A during mid-ebb (experiment A3). Dye concentration (or source water concentration) at grid cells is one when released at the mouth and decreases as it is mixed with nonsource water. Surface concentrations (panels a, b and c) display the accumulation of dye behind the front in the 'core' of the plume the region offshore and slightly rotated downcoast following the path of fresh water (Hetland and MacDonald, 2008). The plume spreads radially early in ebb, but the front becomes asymmetric and bulges in the core of the plume by mid-ebb. The dye depth structure (panels d, e, and f) shows that the tail of a dye patch moves slower than dye at the surface because of the sheared current structure in the plume. The vertical structure of the first release at high water (pink) shows the plunge of the frontal head and wake of downwelled water trailing the front. The dye depth is a reasonable representation of the plume depth, ranging from >5 m at the front to  $\sim$ 2 m behind the front, which compares favorably to observations.

It takes several hours for source water to travel through the plume as it grows, and only the first dyes released interact with the front during the evolving tidal plume stage. Source water-front interaction is also limited spatially; the first dye and surface drifters released spread radially and interact with the front in all directions, but the subsequent releases follow the core of the plume along the central axis such that less source water interacts with the upcoast and downcoast portion of the front. This behavior may be expected, as lateral density gradients weaken as the plume body fills with fresh water. These trends are consistent across the ebbs investigated.

Dye releases are performed with higher temporal resolution in experiment A12. We calculate dye concentration weighted mean plume properties for twelve dyes released in 30 min blocks over tide A. Initially, dye releases freshen, deepen and increase speed during earlymid ebb along with the tidal discharge. Mean dye concentration in the region of frontal convergence is evaluated. Dye concentration in grid cells within a 300 m radius of the front are averaged. O'Donnell et al. (2008) and Horner-Devine et al. (2013) show a frontal decay scale on the order of 15-30 m in plumes of similar scale. Other studies find that the trailing frontal mixing zone can extend hundred of meters into the plume (e.g. Luketina and Imberger (1987)). The goal here is to characterize the region of water that overtakes the front, that may represent a much broader region than the length scale associated with active mixing processes at the front - e.g., the Itsweire length scale,  $L_I = 5u_f/N$ , where  $u_f$  is the frontal propagation speed and N is the buoyancy frequency, as discussed by O'Donnell et al. (2008), typically on the order of 10 m. Mean dye concentration in this estimated frontal 'zone' is evaluated by

$$C_{frontal \ zone} \ t) = \frac{frontal \ zone \ dye \ x \ y \ z \ t) dx dy dz}{frontal \ dx dy dz}. \tag{3}$$

where x, y, z and t are east–west coordinate, north–south coordinate, vertical coordinate and time variables respectively and *dye* is the source water concentration.

Most dye released late in ebb does not reach the front until nearly the beginning of the next ebb, and by this time the front is one of many discharge fronts in the far-field. The dye exhibiting maximum concentration in the front (in experiment A12) is plotted by release and arrival time in Fig. 7. This result further illustrates that only water released during early ebb strongly interacts with the tidal plume front. We refer to the relationship in Fig. 7 as the 'age relation', showing that new source water replaces old source water in the front following an approximate linear trend.

Interior plume mixing dilutes source water that reaches the front. The frontward flux of source water over ebb,  $Q_{front}$  t), is calculated at

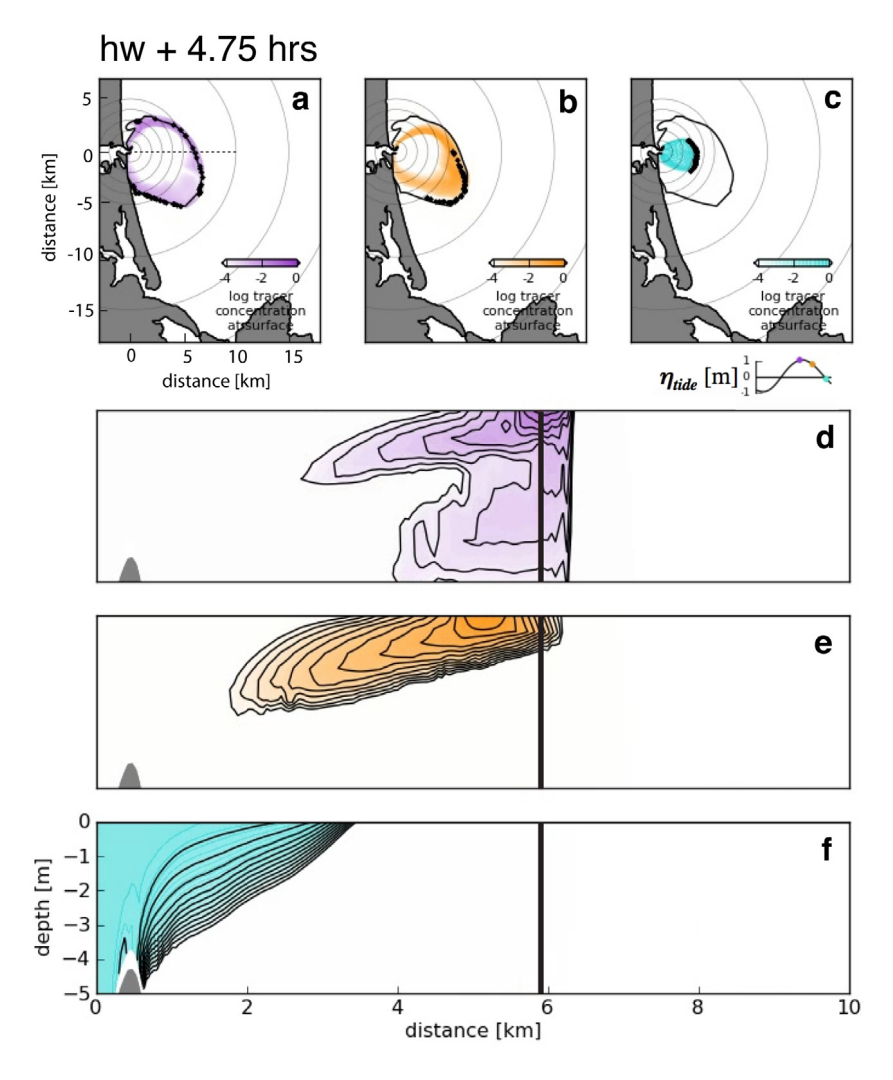
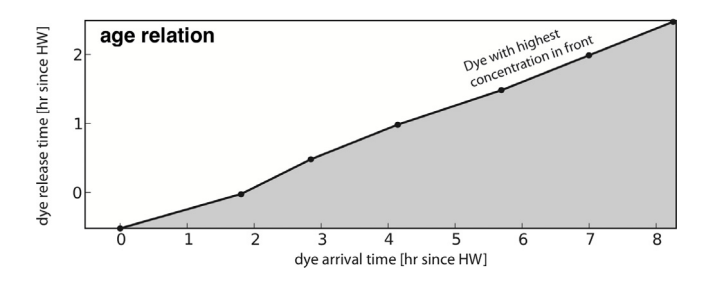


Fig 6 Surface concentration (panels a, b, c) and vertical structure (panels d, e, f) of dyes at max ebb (during tide A labeled in Fig. 3). Dyes are released at times indicated by the matching colored dots on the sea surface height curve in lower right (HW + 0 h, HW + 2 h and HW + 4 h). Panels d, e, f are over transect marked by dotted line in panel a. Black vertical lines in panels d, e, f mark the front distance offshore. Black dots in panels a, b, c show surface drifters released at the mouth with the dye. Black lines in panels a, b, c are front locations.



**Fig** 7 Temporal evolution of dyes with the highest concentration in the front by release time at the mouth and arrival time in the front. Gray shading indicates dyes that have reached the front but are no longer the primary dye present in the frontal zone. 'Arrival time' is calculated in the plume core defined by an angle from 15 to -50 offshore from the mouth in the frontal region (defined over 600 m across the front).

a radius,  $r_{front}$ , 350 m behind the front by

$$Q_{front} t) = \iint_{plume} u_{front} \theta r_{front} z t) dy e \theta r_{front} z t) dS dz$$
 (4)

where  $\theta$  is an angle from the mouth,  $u_{front}$  is the plume radial velocity in the front-following frame (rotated in the  $\theta$  direction), dye is the source water concentration and S  $\theta$   $r_{front}$ ) is a plume arc length. Source water

flux behind the front is evaluated during tide C (experiment C1) with dye released throughout ebb. The plume spreads essentially radially during tide C, facilitating the calculation.

The flux of source water overtaking the front is shown in the top panel of Fig. 8. Model velocities are rotated in the radial direction from the mouth. The plume is divided into 5 angles from the mouth and the mean radial velocity of the front is subtracted from the plume radial velocity field within each angle to investigate plume flow in the front-following frame. Vertical profiles of velocity and source water concentration are used to calculate the radial flux 350 m behind the front. Plume velocity and source water concentration are averaged 300–400 m behind the front resulting in a mean vertical profile in each angle and the flux is calculated assuming an arc length from a circular spreading front. The center panel of Fig. 8 shows the estuarine discharge measured at the mouth.

The bottom panel of Fig. 8 shows the fraction of overtaking source water measured behind the front (panel a) relative to the total estuarine discharge (panel b) released at the same time. The denominator of the metric plotted in panel 'c' is the value shown in panel 'b'; the numerator of the metric plotted in panel 'c' is the value shown in panel 'a' tracked back to time of release, calculated from the age relation (i.e. panel 'a' shifted to time of release on x-axis).

The flux of source water behind the front is an order of magnitude smaller than the ebb discharge because much of the ebbed water

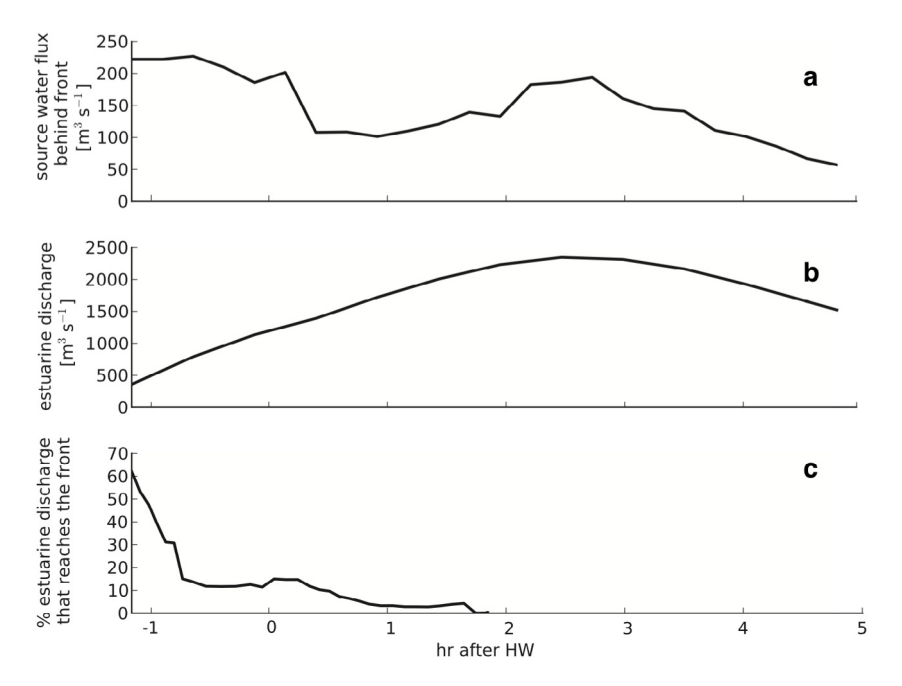


Fig 8 (a) Flux of source water in the front-following frame following the front during tide C (Fig. 3). (b) Discharge at the estuary mouth during tide C. (c) Percent estuarine discharge that overtakes the front, calculated by tracing the source water flux behind the front (panel a) back in time via the age relation in Fig. 7.

is mixed in the plume body. Early in ebb, a large percentage of source water overtakes the front; overtaking velocities span the entire plume early in its formation but quickly diminish in the interior, also contributing to the small percentages throughout most of ebb.

## 3.2. Does estuarine outflow influence frontal propagation?

We consider the front position in the core of the plume in relation to processes at the mouth. The plume core is defined by the average coordinate of a propagating group of 100 numerical surface drifters released at the mouth at the start of ebb. There is spatial variability in front position throughout the plume, so this simplification is necessary. The response of the tidal plume front when a gate closes at the estuary mouth is investigated over tide A. The gate scenarios are achieved by adding a wall to the grid and re-initializing the new grid during ebb. Wind forcing is eliminated in these cases.

Fig. 9 shows results from experiments with and without a gate. The right panel shows the position of the plume fronts in both cases at 5.69 h after high water. The plume front is defined by the dye concentration gradient. The gate is closed at 0.78 h after high water and no additional water is released from the estuary mouth.

The color contours in the left panel in Fig. 9 show time evolution of normalized sea surface height anomaly along a transect through the core of the plume (dashed line in right panel) in the 'no gate' case. Since the figure illustrates the sea surface over many hours, we have removed the tidal height so that only the discharge sea surface anomaly relative to the tide is shown; this quantity is normalized by the initial sea surface height anomaly before the plume emerges. The position of the plume front along the transect is marked with the black (no gate case) and gray (gate case) lines. The gray horizontal lines show the time the gate closes and when water released at that time would have reached the front, according to the age relation in Fig. 7.

The front response to the gate is not instantaneous. The separation of the fronts between the two cases occurs approximately when the source water blocked by the gate would have arrived at the front, indicating that overtaking velocities are relatively unaffected by the gate and the source water already released is enough to supply the front and sustain its propagation for several hours. This suggests that the front propagates nearly independently of the mouth (as in Jay et al. (2010)), but eventually requires replenishing of younger water to maintain its speed.

#### 4 Discussion

The importance of the front to overall plume structure (Garvine, 1982, 1987) is not completely confirmed by this work, as the transport of plume water after it is mixed through the front is not investigated. However, this study does confirm that process in the plume body and local frontal dynamics are responsible for frontal propagation throughout most of ebb, consistent with MacDonald et al. (2007), Hetland and MacDonald (2008), Hetland (2010) and Jay et al. (2010) that emphasize the dynamics of these regions in plume structure. This work suggests that source discharge, highlighted as a main driver of frontal propagation in Kilcher and Nash (2010), is important during the early formation of the plume front, but diminishes in time. Although not evaluated directly, the importance of frontal mixing to the total mixing of estuarine discharge can be extrapolated from this study. Simply by the diminishing source-front connectivity over much of ebb shown in this study, the importance of the front to the total mixing of the estuarine discharge must also be small. During early ebb the front is clearly a dynamic feature driving source water mixing and plume structure, but its significance decreases as the plume lifts-off, grows and a dynamic near-field mixing region develops that appears to separate and function independently from the propagating frontal region at the seaward boundary. Previous studies expressing the strong importance of the front to dilution of the total discharge require a definition of a frontal zone (Orton and Jay, 2005; Pritchard and Huntley, 2006; Huguenard et al., 2016), which this work now suggests could also include a connectivity parameter that incorporates the age and origin of water being mixed near the seaward boundary.

As ebb progresses, source-front connectivity decreases. Integrating Fig. 8 panel c, we find  ${\sim}6.5~$  of discharge released over the first six hours of ebb interacts with the front over that time. This metric is the result of summing in time the fraction of the total source water released shown as a percent in the bottom panel of Fig. 8 panel c. Since the fraction of source water that reaches the front decreases to almost zero after  ${\sim}1.75~$ h after high water, the fraction of the total ebb discharge that reaches the front is small.

Much of the water that composes the frontal region is not tagged by dye, suggesting that the front essentially sustains itself after initial formation. Buoyancy can also be supplied to the front through entrainment of relatively fresh ambient or older source water throughout the

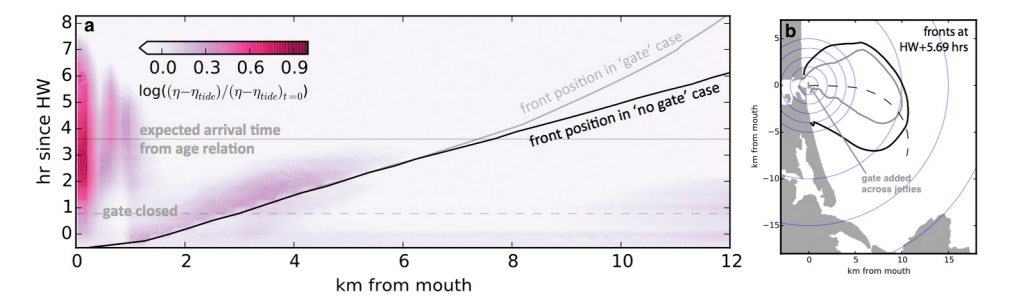


Fig 9 (a) Sea surface anomaly (normalized by the initial pre-plume sea surface anomaly) in the 'no gate' experiment along the transect in panel b. Gray and black lines are the position of the front along the core transect in the 'gate' and 'no gate' experiments. The gray lines indicate when the gate closes (dotted line) and when the blocked source water would have arrived at the front (solid line) in the 'gate' experiment. (b) Position of the plume front at HW + 5.69 h in the 'gate' (gray) and 'no gate' (black) experiments.

plume. When the frontal region is young (i.e., during early ebb), we expect much of the plume water behind the front to overtake the front. As the plume ages, the front decouples from the source. This is not a complete decoupling; all dyes eventually arrive at the front but in increasingly small amounts and well after six hours of ebb. The gate experiments illustrated in Fig. 9 elucidate the independence of the front from processes at the mouth and the length of time the front can sustain itself without a supply of new plume water from the estuary.

This study shows that the mixing and translation of source water though the plume body changes significantly over ebb, indicating that the dynamics of the front likely do as well. Although we do not have the capability to look at the details or number of times source water cycles through the front in this model, the result has significant implications for the mixing and structure of the frontal region, which has not previously been described as a region with significant variability in mixing and structure over the ebb phase of the tide. However, over ebb the front must transition from a small scale propagating discharge front to an intermediate scale shelf front, so these findings are reasonable. Both non-geostrophic (i.e., radial expansion and decreasing barotropic gradients) and geostrophic (i.e., turning of streamlines parallel to the front) processes can contribute to decreasing connectivity between the mouth and front.

Wind and discharge effect plume advection and mixing and will therefore influence source-front connectivity. We have selected tidal cycles during light winds and comparable discharge rates to minimize these confounding influences in our analysis. Wind stress, especially from onshore winds that may cause swell and wave breaking in a field scenario (Gerbi et al., 2013; Thomson et al., 2014) (waves are not modeled here), will mix the plume body and frontal region, and become more influential as the plume grows to increasing surface area. We have selected modeled plumes that spread essentially radially to reduce the wind driven orientation of the front as well as the plume velocities behind it. It is reasonable to assume that in most wind steered plume scenarios, source-front connectivity will decrease relative to these base cases. High river discharge will increase the plume surface area and shear-driven dilution source water experiences as it traverses the plume. It is likely that increasing river discharge will increase source-front connectivity initially as ebb begins, but will then decrease source-front connectivity later in ebb due to increased shear mixing in the more expansive plume interior and the relatively stronger barotropic gradient, g' and velocity at the front compared to these base

Although the connectivity estimate from Fig. 8 panel c is likely influenced by wind and discharge rate and varies somewhat for each ebb, the small percentage suggests that the strong mixing Pritchard and Huntley (2006) and Orton and Jay (2005) measure at the plume front may only be representative of frontal dynamics during a snap shot of ebb. It is reasonable to conclude that early in ebb the front contributes greatly to net mixing of source water, while later in ebb, as the maximum discharge is released, shear mixing of source water in the energetic plume body is greater than frontal mixing (see MacDonald

and Geyer (2004), MacDonald et al. (2007) and Kilcher et al. (2012) on the importance of near-field mixing to plume evolution). As the plume becomes increasingly geostrophic, shear induced mixing associated with the front will transition from velocity shear in the radial direction to velocity shear in the along-front direction, further decreasing the energetics of local mixing processes at the front.

Moreover, since so little of the discharge interacts with the front, these experiments suggest that the front matters less than previously thought to the mixing of the total ebb discharge. In comparison, shear mixing in the near-field becomes increasingly significant with increasing ebb velocities; several ebbs shown in Fig. 4 demonstrate that the water overtaking the front is the same salinity of the front or saltier.

As the front transitions beyond the lift-off region, the flattening of the barotropic surface profile across the plume core can reduce source-front connectivity. Fig. 9 illustrates sea surface height anomaly along a plume core transect between the mouth and the front in the base case without a gate. High sea surface height is sustained at the mouth, increasing over ebb, and behind the front, extending into the plume several kilometers. There is a growing region of low, essentially constant, sea surface height separating the mouth and front regions. As the plume evolves, this growing distance between the highly energetic liftoff region and the radial expansion of the plume front results in a flattening of the surface gradient that disconnects the frontal region from the plume core, and leads to a broad, diffuse region of surface divergence far behind the front. This mechanism of diminishing connectivity is illustrated in Fig. 10. Note that a hydrostatic model is limited in its ability to resolve details of the front and the associated trailing region of frontal interaction; dye tracer averages over large swaths of the frontal region are reasonable, but in-depth dynamic analysis of connectivity is left for future work with a non-hydrostatic model.

The response of the front to the gate experiments (closed during early ebb) indicate that the formation of the frontal region during early ebb influences steady propagation. But even then, Fig. 9 shows that after ~6 h of ebb, the difference in position of the fronts in the core of the plume is similar with and without damming the discharge. The front continues to propagate offshore for several hours before it slows, when it finally experiences the absence of the estuarine discharge blocked by the gate. There is no immediate response in frontal propagation when the gate is closed; thus early ebb estuarine discharge influences frontal propagation, but with a lag. Throughout ebb, with or without a gate, it is plausible that the front propagation in the core is sustained by the local barotropic gradient at the front extending into the plume. The gate appears to affect the lateral scale of the plume more than the cross-shore extent, with later ebb gate closings (not shown) only slightly affecting the lateral plume scale within a few kilometers of the estuary mouth.

## 5 Conclusion

The numerical simulations in this study address the communication between the estuary mouth and the tidal plume front. The translation

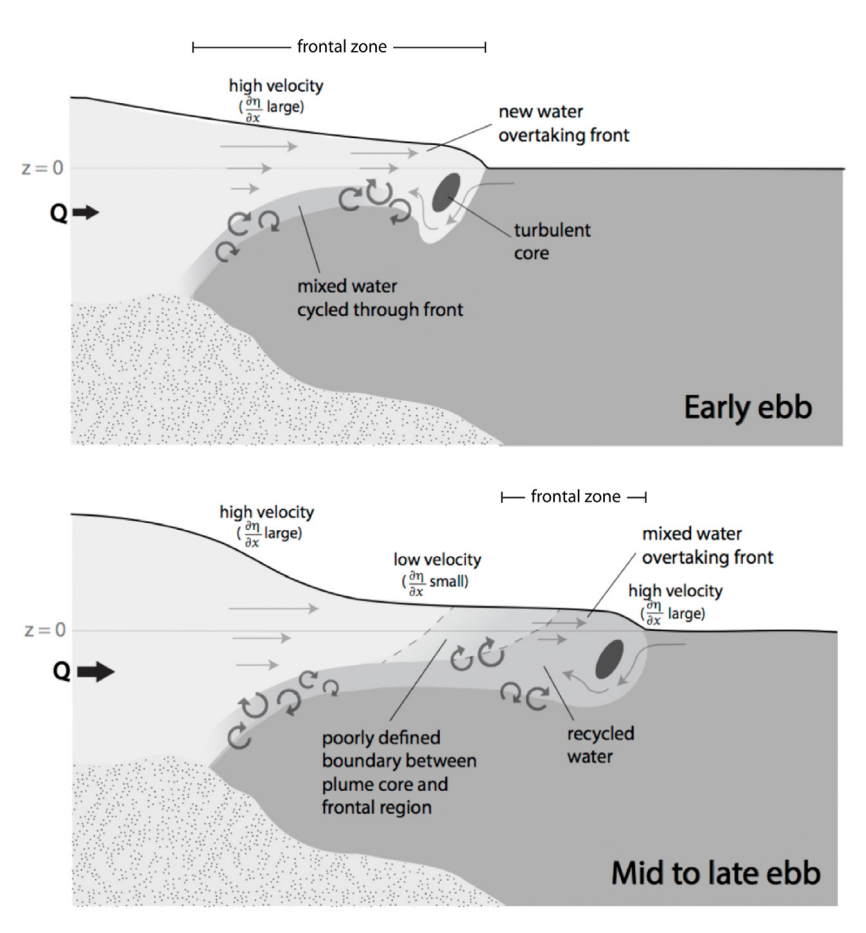


Fig 10 Frontal evolution over ebb. Early ebb panel shows the frontal region scales with the entire plume and a significant fraction of source water is processed through the front. Mid to late ebb panel shows separation of the frontal region from the source and the development of an interior region where diluted plume water with weak overtaking velocities travels frontward.

of source water through the plume is examined; the amount of source water that reaches the front over a single ebb is quantified and the role of time dependent estuarine discharge on frontal propagation is investigated.

The main conclusion of this study is that much of the total discharge released over an ebb pulse does not interact with the propagating tidal plume front. River plume source-front connectivity diminishes over ebb and the front essentially decouples from the source and sustains itself as a distinct water mass. Local frontal dynamics Jay et al. (2010) and processes in the plume body MacDonald et al. (2007) are responsible for the advancement of the plume. Communication with the source (Kilcher and Nash, 2010) is less important, outside of early plume formation. These experiments suggest that the growing distance between the mouth region and the plume front results in a flattening of the surface gradient driving flow in the interior, diminishing source-front connectivity.

# Declaration of competing interest

The authors declare that they have no known competing financial interests or personal relationships that could have appeared to influence the work reported in this paper.

#### CRediT authorship contribution statement

Kelly L Cole: Conceptualization, Analysis, Writing, Editing. Daniel G MacDonald: Conceptualization, Analysis, Writing, Editing, Data curation, Project management. Georgia Kakoulaki: Data curation, Writing, Editing. Robert D Hetland: Project management, Funding acquisition.

### Acknowledgments

This work is funded by National Science Foundation, USA awards 1756690, 1756599, 0850622 and 0850948.

#### References

Benjamin, T., 1968. Gravity currents and related phenomena. J. Fluid Mech. 31, 209–248.

Canuto, V., Howard, A., Cheng, Y., Dubovikov, M., 2001. One-point closure model momentum and heat vertical diffusivities. J. Phys. Oceanogr. 31, 1413–1426.

Chen, J.C., 1980. Studies on Gravitational Spreading Currents (Ph.D. thesis). California Institute of Technology, Pasadena, CA.

Chen, F., MacDonald, D., 2006. Role of mixing in the structure and evolution of a buoyant discharge plume. J. Geophys. Res. 111 (C11002), http://dx.doi.org/10. 1029/2006JC003563.

Chen, F., MacDonald, D., Hetland, R., 2009. Lateral spreading of a near -field river plume: Observations and numerical simulations. J. Geophys. Res. 114 (C07013), http://dx.doi.org/10.1029/2008JC004893.

Cole, K., 2014. A Numerical Study of the Mid-Field River Plume (Ph.D. thesis). Texas A and M University.

Flater, D., 2005. Xtide version 2.8.2. URL: https://flaterco.com/xtide/.

Flather, R., 1976. A tidal model of the northwest european continental shelf. Mem. Soc. R. Sci. Liege 10 (6), 141–164.

Garvine, R., 1982. A steady state model for buoyant surface plume hydrodynamics in coastal waters. Tellus 34, 293–306.

Garvine, R., 1987. Estuary plumes and fronts in shelf waters: A layer model. J. Phys. Oceanogr. 17, 1877–1896.

Garvine, R.W., Monk, J.D., 1974. Frontal structure of a river plume. J. Geophys. Res. 79 (15), 2251–2259.

Gerbi, G.P., Chant, R.J., Wilkin, J.L., 2013. Breaking surface wave effects on river plume dynamics during upwelling-favorable winds. J. Phys. Oceanogr. 43 (9), 1959–1980.

Geyer, W.R., Scully, M.E., Ralston, D.K., 2008. Quantifying vertical mixing in estuaries. Environ. Fluid Mech. 8 (5–6), 495–509.

- Geyer, W., Signell, R., Fong, D., Wang, J., Anderson, D., Keafer, B., 2004. The freshwater transport and dynamics of the western Maine coastal current. Cont. Shelf Res. 24 (12), 1339–1357.
- $\label{eq:Hetland} Hetland, R., 2005. Relating river plume structure to vertical mixing. J. Phys. Oceanogr. \\ 35, 1667–1688. \\ http://dx.doi.org/10.1175/JPO2774.1.$
- Hetland, R., 2010. The effects of mixing and spreading on density in near-field river plumes. Dyn. Atmos. Oceans 49 (1), 37–53. http://dx.doi.org/10.1016/j.dynatmoce. 2008.11.003.
- Hetland, R., MacDonald, D., 2008. Spreading in the near-field Merrimack River plume. Ocean Modell. 21, 12–21. http://dx.doi.org/10.1016/j.ocemod.2007.11.001.
- Horner-Devine, A.R., Chickadel, C.C., MacDonald, D.G., 2013. Coherent structures and mixing at a river plume front. In: Coherent Flow Structures at Earth's Surface. Wiley Online Library, pp. 359–369.
- Horner-Devine, A.R., Hetland, R.D., MacDonald, D.G., 2015. Mixing and transport in coastal river plumes. Annu. Rev. Fluid Mech. 47, 569–594.
- Huguenard, K., Bogucki, D., OrtizSuslow, D., Laxague, N., MacMahan, J., Özgökmen, T., Haus, B., Reniers, A., Hargrove, J., Soloviev, A., Graber, H., 2016. On the nature of the frontal zone of the choctawhatchee bay plume in the gulf of Mexico. J. Geophys. Res.: Oceans 121 (2), 1322–1345.
- Huppert, H.E., Simpson, J.E., 1980. The slumping of gravity currents. J. Fluid Mech. 99 (4), 785–799.
- Jay, D.A., Zaron, E.D., Pan, J., 2010. Initial expansion of the Columbia River tidal plume: Theory and remote sensing observations. J. Geophys. Res. 115 (C00B15), http://dx.doi.org/10.1029/2008JC004996.
- Kilcher, L.F., Nash, J.D., 2010. Structure and dynamics of the Columbia River tidal plume front. J. Geophys. Res. 115 (C05S90), http://dx.doi.org/10.1029/ 2009 C006066
- Kilcher, L.F., Nash, J.D., Moum, J.N., 2012. The role of turbulence stress divergence in decelerating a river plume. J. Geophys. Res. 117 (C5).
- Lowe, R.J., Linden, P., Rottman, J.W., 2002. A laboratory study of the velocity structure in an intrusive gravity current. J. Fluid Mech. 456, 33–48.
- Luketina, D.A., Imberger, J., 1987. Characteristics of a surface buoyant jet. J. Geophys. Res. 92 (C5) 5435–5447
- MacDonald, D., Geyer, W., 2004. Turbulent energy production and entrainment at a highly stratified estuarine front. J. Geophys. Res. 109 (C05004), http://dx.doi.org/ 10.1029/2003JC002094.

- MacDonald, D., Goodman, L., Hetland, R., 2007. Turbulent dissipation in a near-field river plume: A comparison of control volume and microstructure observations with a numerical model. J. Geophys. Res. 112 (C07026), http://dx.doi.org/10.1029/ 2006JC004075.
- Marino, B., Thomas, L., Linden, P., 2005. The front condition for gravity currents. J. Fluid Mech. 536, 49–78.
- Marmorino, G.O., Trump, C.L., 2000. Gravity current structure of the Chesapeake Bay outflow plume. J. Geophys. Res. 105 (C12), 28847–28861. http://dx.doi.org/10. 1029/2003JC002094.
- O'Donnell, J., Ackleson, S.G., Levine, E.R., 2008. On the spatial scales of a river plume. J. Geophys. Res.: Oceans 113 (C4).
- O'Donnell, J., Marmorino, G., Trump, C., 1998. Convergence and downwelling at a river plume front. J. Phys. Oceanogr. 28, 1481–1495.
- Orlanski, I., 1976. A simple boundary condition for unbounded hyperbolic flows. 21, pp. 251–269.
- Orton, P., Jay, D., 2005. Observations at the tidal plume front of a high-volume river outflow. Geophys. Res. Lett. 32 (L11605), http://dx.doi.org/10.1029/2005GL022372.
- Pritchard, M., Huntley, D., 2006. A simplified energy and mixing budget for a small river plume discharge. J. Geophys. Res. 111 (C03019), http://dx.doi.org/10.1029/ 2005.IC002984.
- Ralston, D.K., Geyer, W., Lerczak, J.A., 2010. Structure, variability, and salt flux in a strongly forced salt wedge estuary. J. Geophys. Res. 115 (C6).
- Rottman, J.W., Simpson, J.E., 1983. Gravity currents produced by instantaneous releases of a heavy fluid in a rectangular channel. J. Fluid Mech. 135, 95–110.
- Scotti, A., Pineda, J., 2007. Plankton accumulation and transport in propagating nonlinear internal fronts. J. Mar. Res. 65, 117–145.
- Shchepetkin, A., McWilliams, J., 2005. The regional oceanic modeling system (ROMS):
  A split-explicit, free-surface, topography-following-coordinate oceanic model. Ocean Modell. 9 (4), 347–404.
- Smolarkiewicz, P., Clark, T., 1986. The multidimensional positive definite advection transport algorithm: further development and applications. J. Comp. Phys. 67 (2), 396–438
- Thomson, J., HornerDevine, A.R., Zippel, S., Rusch, C., Geyer, W., 2014. Wave breaking turbulence at the offshore front of the columbia river plume. Geophys. Res. Lett. 41 (24), 8987–8993.
- Yankovsky, A., Chapman, D., 1997. A simple theory for the fate of buoyant coastal discharges. J. Phys. Oceanogr. 27, 1386–1401. http://dx.doi.org/10.1175/ 15200485(1997)027<1386:ASTFTF>2.0.CO;2.